Method for the navigation line recognition of the ridge without crops via machine vision

Wei Liu, Jianping Hu*, Jiaxin Liu, Rencai Yue, Tengfei Zhang, Mengjiao Yao, Jing Li
(*School of Agricultural Engineering, Jiangsu University, Zhenjiang 212013, Jiangsu, China*)

Abstract: Some agriculture machinery like the transplanter, needs to operate by following the crop-free ridges. In order to improve working efficiency and quality, some autonomous navigation systems were developed and applied to ridge-following machinery. At present, agricultural navigation systems are mainly the satellite navigation system and the machine vision system. The satellite navigation system is difficult to apply to the machinery that needs to work by following the ridge because it cannot distinguish the shape of the navigated ridge and guide the machinery working along the ridge. In this study, 697 cloudy ridge images and 235 sunny ridge images were taken in the field, and these images were used as the dataset. Moreover, a machine vision navigation method based on the color of ridges was proposed. Firstly, the regions of interest (ROI) in the ridge image were extracted according to the reaction time and the forward speed of the machine. Then, a gray reconstruction method was used to enlarge the color difference between the ridge and the furrow. The optimal threshold for the gray image segmenting was calculated real-timely by using the threshold segmentation method. Then, based on the contour detection method, the ridge contour which was not surrounded by holes was extracted. Finally, the approximate quadrilateral method was proposed to recognize the ridge center line as the navigation line. The method proposed in this study was verified by four types of ridges with different colors and textures. The experimental results showed that the recognition success rates of the light ridge, the dark ridge, the film-covered ridge, and the sunny ridge were 100%, 97.5%, 100%, and 98.7%, respectively. The recognition success rate of the proposed method was at least 8% higher than that of the existing ridge-furrow recognition methods. The results indicate that this method can effectively realize navigation line recognition. This method can provide technical support for the autonomous navigation of agricultural machinery, such as transplanters, seeders, etc., operating on the ridge without crops.

Keywords: navigation line recognition, machine vision, ridge line recognition, intelligent agriculture
DOI: 10.25165/j.ijabe.20241702.7480

Citation: Liu W, Hu J P, Liu J X, Yue R C, Zhang T F, Yao M J, et al. Method for the navigation line recognition of the ridge without crops via machine vision. Int J Agric & Biol Eng, 2024; 17(2): 230–239.

1 Introduction

Ridge farming is a farming method that arranges ridges and furrows in parallel along the long side of farmland. This farming method can expand soil surface area, improve soil ventilation, and improve light transmittance[1]. It is widely used in planting potatoes[2], strawberries[3], green vegetables[4,5], maize[6,7], soybeans, trees and other roadside crops. The machinery used to plant the above roadside crops needs to follow the ridge during operations. The bending of the ridge often occurs due to artificially controlled ridging. The satellite positioning and navigation system is fixed trajectory navigation[8,9] and is unable to detect whether the ridge is bent and the bending degree of the ridge. Therefore, it is not suitable for the machinery working on ridges. The machine vision navigation system can collect and process ridge images in real-time and extract the navigation line[10,11], so it is more in line with the actual requirements of operation in the ridge farming environment.

At present, most of the researches on the recognition method of navigation line are to extract the crop rows as the navigation line when there are crops on the ridge. For example, Ospina et al.[12] used the threshold function and the morphological operation to accurately segment the crop rows, and then used the minimum square method to extract the crop line as the navigation line of harvesting and plant protection machinery operating on ridges. Chen et al.[13] used the Otsu method to segment crops and furrows based on the RGB color space, and proposed the prediction point Hough transform method to identify the furrow center line between crops as the navigation line of the picking robot. In addition, Rabab et al.[14] and Hamuda et al.[15] also used the color difference between crops and soil to segment the crop rows from the soil and used the crop rows as the navigation line when the machinery worked on ridges.

However, some agricultural machinery, such as the transplanter and the seeder, are on crop-free ridges, so it is necessary to recognize the navigation line for the ridge without crops. There is no obvious color difference between the furrow and the ridge so the existing studies mostly used the shadow information between the ridge and the furrow under the outdoor sunlight to recognize the furrow line. For example, Morio et al.[16] used the color-based

Received date: 2022-03-21 **Accepted date:** 2023-05-27
Biographies: Wei Liu, PhD, Assistant Researcher, research interest: control theory and technology of intelligent agricultural equipment, Email: Mario_liu@ujs.edu.cn; **Jiaxin Liu**, Master candidate, research interest: computer vision, Email: xianmoyisheng@163.com; **Rencai Yue**, Doctoral candidate, research interest: intelligent agricultural equipment design theory and technology, Email: YRC19920318@163.com; **Tengfei Zhang**, Doctoral candidate, research interest: intelligent agricultural equipment design theory and technology, Email: tengfeizhang2021@163.com; **Mengjiao Yao**, Master candidate, research interest: theory and application of intelligent agricultural equipment control, Email: 2221916042@stmail.ujs.edu.cn; **Jing Li**, Master candidate, research interest: mechanical modeling and simulation. Email: 18860874285@163.com.
***Corresponding author: Jianping Hu**, PhD, Professor, research interest: intelligent agricultural equipment design theory and application. School of Agricultural Engineering, Jiangsu University, Zhenjiang 212013, Jiangsu, China. Tel: +86-13852984643, Email: hujp@ujs.edu.cn.

furrow detection filter to recognize furrow lines. This filter used the characteristic of a large color difference between the furrow and the ridge in the outdoor ridge image. The recognition results showed that for the image with multiple ridges in the field of view, the recognition success rate was more than 90%. For the images with only three or fewer ridges in the field of view, the recognition success rate was 86.9%, and the image with a small color difference between the furrow and the ridge cannot recognize the furrow line. Takagaki et al.[17] recognized the furrow center line of the image with shadow under the sun by recognizing the position of the shadow boundary line and the known ridge width information. The recognition success rate of this method was 100%, but it was not suitable for the image without shadow. In addition, Takagaki et al. also used the characteristics of complex ridge texture and uniform furrow texture to segment ridge and furrow and used the Hough transform to recognize the furrow line. The recognition success rate of this method was 87%, and it could only recognize the ridge image with the above texture features.

Due to the different soil types, soil humidity, light intensities, and ridging methods[18], the color and texture of ridges are complex and diverse. The above methods can only recognize furrow lines according to the characteristics of the ridge image in a specific working environment, so the applicability and robustness of the method are not acceptable. Therefore, the study presented in this paper proposed a navigation line recognition method based on ridge color. In this method, a gray reconstruction method was used to enlarge the small color difference between the ridge and the furrow in the image. The threshold segmentation method, which had autonomic computing features, was used to calculate the optimal threshold for the gray image segmenting in real-time. This threshold segmentation method made the navigation line recognition method proposed in this paper suitable for different color ridges. In this study, a contour detection method, which had the topological analysis ability, was used to detect the ridge contour. This contour detection method can only detect the external contour whose boundary was not surrounded by holes. Therefore, the influence of holes on the ridge on contour detection could be reduced. Finally, the approximate quadrilateral method recognized the ridge center line according to the ridge contour and took the ridge center line as the navigation line. The approximate quadrilateral method can still recognize the ridge center line when the ridge contour lacked boundary but the texture feature was obvious. Therefore, this method made the navigation line recognition method suitable for different texture ridges. In this study, four types of ridge images (the light ridge, the dark ridge, the film-covered ridge, and the sunny ridge) were used to verify the applicability of the navigation line recognition method for different ridges.

The objectives of this study are listed as follows:

1) To navigate the machinery operating on the ridges, a navigation line recognition method needs to be developed;

2) The proposed method can recognize the navigation lines of ridges under practical illumination and environmental conditions;

3) In order to meet the actual working condition, the recognition success rate of the proposed navigation line recognition method should be more than 97%, and its running time should be less than 0.3 s.

2 Materials and methods

2.1 Data collection

In order to verify the effectiveness and universality of the navigation line recognition method based on the ridge color proposed in this study. 697 cloudy ridge images and 235 sunny ridge images were taken as the dataset. 697 cloudy ridge images including 262 light ridge images, 171 film-covered ridge images, and 264 dark ridge images. 235 sunny ridge images were collected in the same ridge block, so there was no ridge color discrimination in sunny ridge images. The collection place of the cloudy ridge images was in Rudong Modern Agricultural Industrial Park, Jiangsu Province, China. The collection place of the sunny ridge images was in Shiyezhou, Zhenjiang City, Jiangsu Province, China. The collection equipment is a Hikvision (China) monocular camera, the model is MV-CH120-10GC. The specific parameters of the camera are listed in Table 1.

Table 1 Parameters of the camera used in the experiment

Name	Parameter
Highest resolution	4096×3000
Frame rate	9.4 fps
Pixel size	3.45 μm×3.45 μm
Sensor type	CMOS
Target size	1.1 inch
Data interface	Gige

The camera was installed in front of the central axis of the transplanter, as shown in Figure 1. The forward speed of the transplanter was about 1.3 km/h. The acquisition mode of the ridge image is continuous acquisition at 9.4 fps during the advancement of the transplanter.

Figure 1 Camera installation location

The light ridge images, film-covered ridge images, and sunny ridge images were near-field collections, the camera installation height was 1.5 m, and the included angle with the horizontal line was 60°.

The dark ridge images were a far-field collection, the camera installation height was 1.5 m, and the included angle with the horizontal line was 45°.

The processor of the hardware device used in the image processing was Intel Core i5 whose main frequency was 2.4 GHz. The memory of the processor was 8 GB and the operating system was Windows 10. The navigation line recognition method program was developed by Microsoft Visual Studio 2019 and OpenCV 4.4.

2.2 Image preprocessing method

The navigation line recognition method first extracted the static regions of interest (ROI) according to the reaction time and the forward speed of the machine. Then, a gray reconstruction method was used to transform the original image in the ROI into the gray image. The optimal threshold for the current gray image segmenting was calculated in real-time and the gray image was transformed into the binary image by using the threshold segmentation method. Then, the external contours in the binary image were extracted

based on the contour detection method. The ridge surface contour in the external contours was filtered by the maximum area method. Based on the ridge surface contour, an approximate quadrilateral method was proposed to extract the ridge center line as the navigation line of the machinery operating on the ridge without crops.

This method is divided into the following parts: 1) Image preprocessing method; 2) Threshold segmentation method; 3) Contour detection method; 4) Ridge center line extraction method. The flow chart of this method is shown in Figure 2.

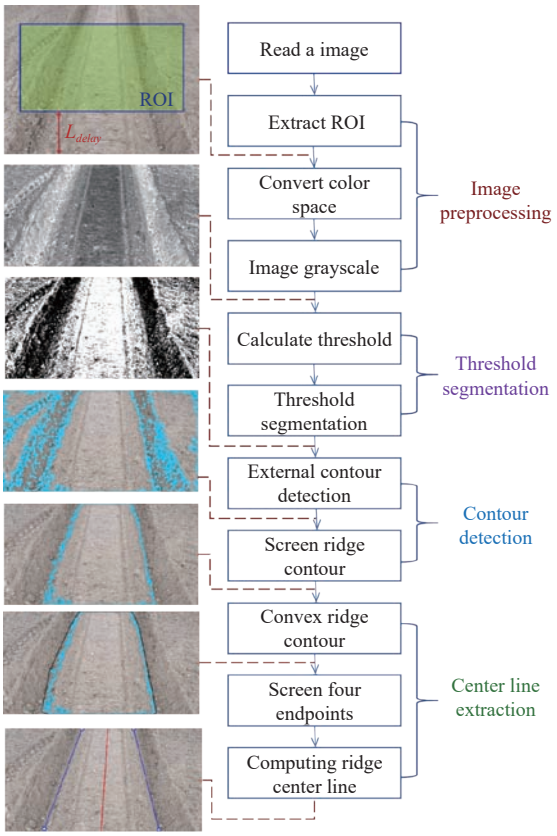

Note: the procedures of the image processing method are listed in the boxes; the red dashes connect the processed procedures and the outcome of the processed pictures.

Figure 2 Flow chart of navigation line recognition method

In Figure 2, the first picture shows the extracted ROI area. The second picture displays the image in grayscale. The third picture shows the segmenting result of the ridge. The fourth picture demonstrates the detection of the external contour. The fifth picture displays the screened ridge contour. The sixth picture illustrates the convex ridge contour. The seventh picture shows the center line of the ridge.

2.2.1 Regions of interest extraction method

Machine vision navigation carries out image acquisition, image processing, and steering control in the process of moving forward. There is a time difference between image acquisition and steering control. The components of time difference are algorithm running time and machine response time. During this time difference, the machine continues to move forward, so there is a problem the recognized navigation line is not the actual navigation line for the machine to make steering response. In addition, due to the large camera vision, the ridge in the image is long and bent. If the ridge recognition is based on the whole image, the recognition error is large and the algorithm runs longer. Therefore, in order to solve the above problems, this study proposed a ROI extraction method. This method calculated the position of the ROI by integrating the algorithm running time, mechanical response time, and mechanical forward speed.

The distance advanced within the delay distance L_{delay} was calculated according to the algorithm running time T_{alg}, mechanical reaction time T_{mech}, and mechanical forward speed v as follows:

$$L_{delay} = \left(T_{alg} + T_{mech}\right) \times v \quad (1)$$

where, L_{delay} is the delay distance of the world coordinate system, m; T_{alg} is the algorithm running time, s; T_{mech} is the mechanical reaction time, s; v is the forward speed of the machine, m/s. The delay distance of the image coordinate system could be calculated through the conversion equation from the world coordinate system to the image coordinate system. The delay distance of the image coordinate system was taken as the distance from the lower boundary of the ROI to the lower boundary of the image.

In order to further reduce the length of the recognized ridge, the height of the ROI was set to 0.6 times the height of the image. In addition, in order to reduce the influence of the background outside the ridge and furrow on the navigation line recognition, the width of the recognition region should be reduced under the condition of ensuring the integrity of the ridge and furrow. So the width of the ROI was calculated using Equation (2).

$$W_{ROI} = k(W_{ridge} + 2W_{furrow}) \quad (2)$$

where, W_{ROI} is the width of the ROI area, m; W_{ridge} is the width of the ridge, m; W_{furrow} is the width of the furrow, m; k is the safety factor which was set to 1.1 in this research.

The schematic diagram of the ROI is shown in Figure 3. The ROI area is the central section of the field of view (FOV). The processing speed would be faster if only the ROI area is processed rather than the whole FOV area.

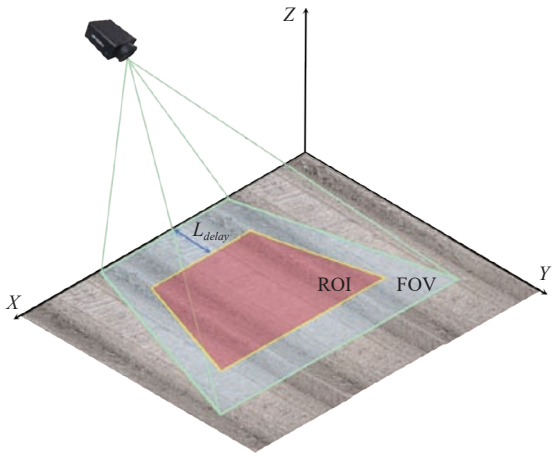

Note: L_{delay} is the delay distance of the world coordinate system. ROI, Region of Interest; FOV, Field of View.

Figure 3 Schematic diagram of a region of interest

2.2.2 Gray reconstruction method

The three elements of color are hue, brightness, and saturation. Because the ridge and the furrow have similar hues, they cannot be distinguished in the hue channel. The color difference between the ridge and the furrow is caused by the brightness difference. The brightness difference is caused by the height difference between the ridge and the furrow. So the brightness was used to distinguish the ridge and the furrow. There are independent brightness channels in HSV, Lab, and YUV color spaces. The V-channel image of HSV

color space, the L-channel image of Lab color space, and the Y-channel image of YUV color space were extracted and compared. The comparison results showed that the pixel values of the three brightness channels (i.e., the V channel of the HSV color space, the L channel of the Lab color space, and the Y channel of the YUV color space) were very similar, as shown in Figure 4. However, the range of the gray values in the V-channel of the HSV color space was the greatest among the three bright channels. Applying a V-channel as the brightness channel would contrast the ridge and furrow relatively strongly. Thus, the HSV color space was used as the image-transforming space.

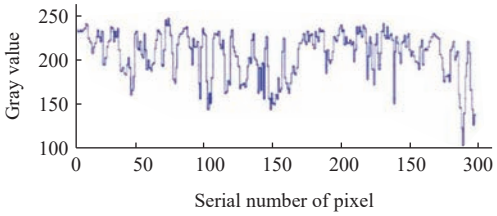

a. Gray values in the V channel of the HSV color space

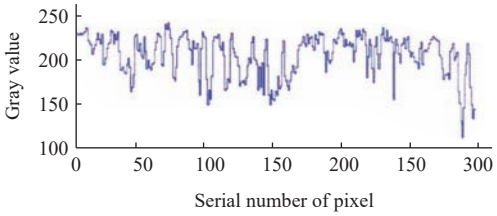

b. Gray values in the L channel of the Lab color space

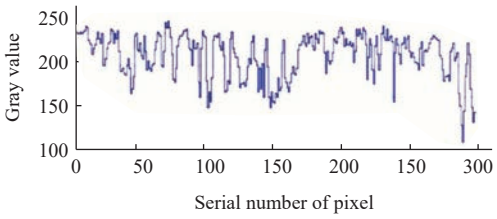

c. Gray values in the Y channel of the YUV color space

Figure 4 Bright components in the HSV, the Lab, and the YUV color spaces

Although V-channel had the greatest range of the pixel value, the brightness difference between the ridge and furrow was still not obvious. In order to increase the difference of pixel values between the ridge and the furrow, the pixel value pix(i, j) of the gray image was set as,

$$\mathrm{pix}(i,j) = 2 \times \mathrm{pixv}(i,j) \tag{3}$$

where, pixv(i, j) means the pixel value of the V channel; pix(i, j) indicates the pixel value of the gray image.

Due to the most of pixv(i, j) were greater than 128, most of the pix(i, j) were greater than the maximum pixel value of 255. The image pixel value rule is listed as follows:

$$\mathrm{pix}(i,j) = \begin{cases} \mathrm{pix}(i,j), & \mathrm{pix}(i,j) < 255 \\ 255, & \mathrm{pix}(i,j) \geq 255 \end{cases} \tag{4}$$

If pix(i, j)=2·pixv(i, j), the original pixel relationship would be changed, so it would be reset as,

$$\mathrm{pix}(i,j) = 2 \times \left(255 - \mathrm{pixv}(i,j)\right) \tag{5}$$

On the basis of keeping the original image relationship as much as possible, the purpose of increasing the pixel difference between ridge and furrow was also achieved.

2.3 Threshold segmentation method

Due to the different soil quality and lighting environment, the pixel values of the ridge in different ridge images are also different. Fixed value threshold segmentation cannot be applied to the ridges with different colors. At present, there are two kinds of threshold segmentation methods for autonomously calculating threshold. One is the global threshold segmentation method and the other is the local adaptive threshold segmentation method. The Otsu method[19] is a global threshold segmentation method and the Sauvola method[20] is a local adaptive threshold segmentation method. The Otsu method and the Sauvola method were used to segment the gray image respectively, and the binary images are shown in Figure 5.

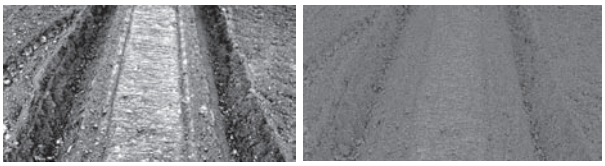

a. Otsu method b. Sauvola method

Figure 5 Examples of binary image outputs of two segmentation methods

The local adaptive threshold segmentation was not suitable for ridge and furrow segmentation. There were countless small holes on the ridge and furrow, and the pixel value of the small holes in the gray image was the highest. The Otsu method used the pixel value of the whole image to calculate the threshold value which was affected by the small holes, and could not segment the ridge and furrow, as shown in Figure 5a. The local adaptive threshold segmentation method calculates the threshold suitable for segmenting each small region. Therefore, the binary image obtained by the Sauvola method showed the texture of the soil, as shown in Figure 5b. Therefore, a global threshold segmentation method using the pixel values of the ridge and furrow to calculate the threshold was proposed in this study.

Because the camera used to collect images was installed in front of the central axis of the machine, the ridge was located in the middle of the image. Due to the imaging principle of near large and far small, the ridge width at the bottom of the image is the largest. At the same time, the error between the center point of the ridge at the bottom of the image and the center point of the image is the smallest. For the above reasons, a 40×40 pixels matrix at the center of the bottom of the image was extracted as an ideal ridge pixel matrix. The range of the pixel matrix was $\left(\frac{W_{\mathrm{img}}}{2} - 20, \frac{W_{\mathrm{img}}}{2} + 20\right]$, and the average pixel value was calculated and recorded as $\overline{\mathrm{pix}}_{\mathrm{rmid}}$, where W_{img} is the width of the image.

The ridge width of the image edge (W_{ridge}) was known. According to the image center position and ridge width, the ideal furrow position could be determined. The range of the pixel matrix on the ideal furrow was $\left(\frac{W_{\mathrm{img}}}{2} + \frac{W_{\mathrm{ridge}}}{2} - 20, \frac{W_{\mathrm{img}}}{2} + \frac{W_{\mathrm{ridge}}}{2} + 20\right]$ and the average pixel value was calculated and recorded as $\overline{\mathrm{pix}}_{\mathrm{fmid}}$.

Due to the image acquisition in the process of moving, there is a deviation between the ridge center point and the image center point. The calculated furrow position may not be the real furrow position. In order to find the real furrow position, it is necessary to take a pixel matrix on both sides of the calculated furrow position. The range of the pixel matrix on the left side of the calculated furrow was $\left(\frac{W_{\mathrm{img}}}{2} + \frac{3W_{\mathrm{ridge}}}{8} - 20, \frac{W_{\mathrm{img}}}{2} + \frac{3W_{\mathrm{ridge}}}{8} + 20\right]$, and the

average pixel value was calculated and recorded as $\overline{\text{pix}}_{\text{fleft}}$; The range of the pixel matrix on the right side of the calculated furrow was $\left(\frac{W_{\text{img}}}{2}+\frac{5W_{\text{ridge}}}{8}-20, \frac{W_{\text{img}}}{2}+\frac{5W_{\text{ridge}}}{8}+20\right]$, and the average pixel value was recorded as $\overline{\text{pix}}_{\text{fright}}$.The position distribution of the ridge pixel matrix and furrow candidate pixel matrix are shown in Figure 6.

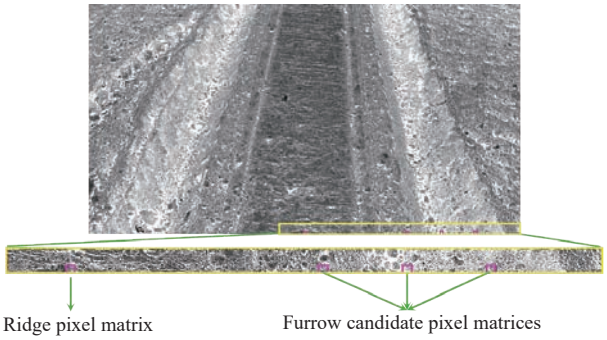

Figure 6 Schematic diagram of small pixel block position

Compared $\overline{\text{pix}}_{\text{fmid}}$, $\overline{\text{pix}}_{\text{fleft}}$, $\overline{\text{pix}}_{\text{fright}}$ with $\overline{\text{pix}}_{\text{rmid}}$ respectively, and calculated the difference value:

$$\Delta\overline{\text{pix}}_{\text{fmid}} = \left|\overline{\text{pix}}_{\text{fmid}} - \overline{\text{pix}}_{\text{rmid}}\right| \quad (6)$$

$$\Delta\overline{\text{pix}}_{\text{fleft}} = \left|\overline{\text{pix}}_{\text{fleft}} - \overline{\text{pix}}_{\text{rmid}}\right| \quad (7)$$

$$\Delta\overline{\text{pix}}_{\text{fright}} = \left|\overline{\text{pix}}_{\text{fright}} - \overline{\text{pix}}_{\text{rmid}}\right| \quad (8)$$

Compare the values of $\Delta\overline{\text{pix}}_{\text{fmid}}$, $\Delta\overline{\text{pix}}_{\text{fleft}}$, and $\Delta\overline{\text{pix}}_{\text{fright}}$ find the maximum value. If $\Delta\overline{\text{pix}}_{\text{fmid}}$ is the maximum, the thres = $\frac{\overline{\text{pix}}_{\text{rmid}}+\overline{\text{pix}}_{\text{fmid}}}{2}$; If $\Delta\overline{\text{pix}}_{\text{fleft}}$ is the maximum, the thres = $\frac{\overline{\text{pix}}_{\text{rmid}}+\overline{\text{pix}}_{\text{fleft}}}{2}$; If $\Delta\overline{\text{pix}}_{\text{fright}}$ is the maximum, the thres = $\frac{\overline{\text{pix}}_{\text{rmid}}+\overline{\text{pix}}_{\text{fright}}}{2}$.

In order to ensure that the pixel value of the ridge after threshold segmentation was 255, it was necessary to compare the values of $\overline{\text{pix}}_{\text{rmid}}$ and *thres*. The specific segmentation rules were shown as follows:

$$\text{If } \overline{\text{pix}}_{\text{rmid}} < thres,\ \text{pix}(i,j) = \begin{cases} 0, & \text{pix}(i,j) \geq \text{thres} \\ 255, & \text{pix}(i,j) < \text{thres} \end{cases}.$$

$$\text{If } \overline{\text{pix}}_{\text{rmid}} > thres,\ \text{pix}(i,j) = \begin{cases} 0, & \text{pix}(\text{i,j}) < \text{thres} \\ 255, & \text{pix}(\text{i,j}) \geq \text{thres} \end{cases}.$$

2.4 Contour detection method

There were many independent small pixel blocks and irregular textures connected by countless small pixel blocks in the binary image, as shown in Figure 7. Therefore, the boundary detected by Canny method[21] is the boundary of countless small holes, not the ridge boundary, as shown in Figure 8.

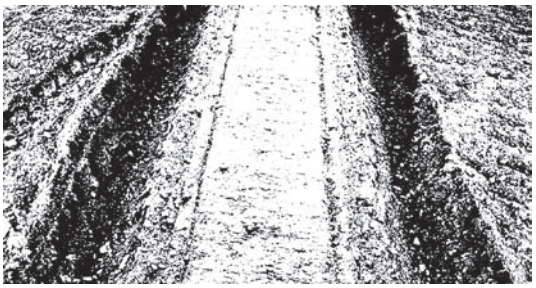

Figure 7 An example of binary images

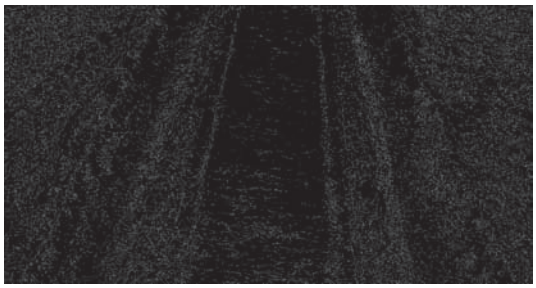

Figure 8 An example of Canny method boundary detection results

In order to eliminate the influence of holes on the ridge on the detection of ridge boundary, a boundary detection method[22], which had the topological analysis ability, was used in this study. This method can mark the boundary as a contour or hole while detecting the boundary, and generate the hierarchical information of all boundaries, as shown in Figure 9.

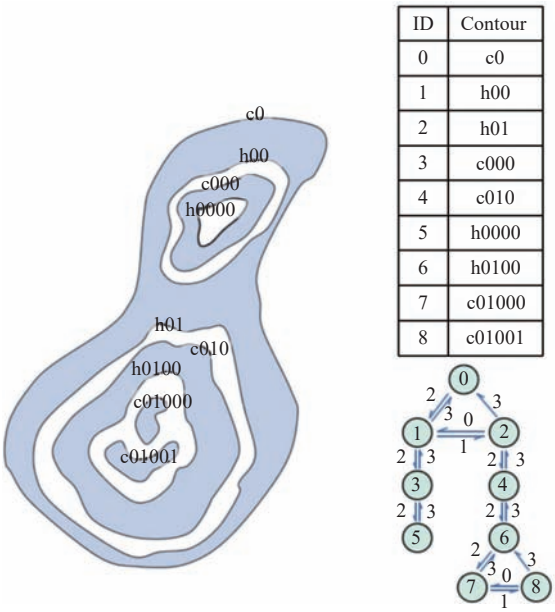

ID	Contour
0	c0
1	h00
2	h01
3	c000
4	c010
5	h0000
6	h0100
7	c01000
8	c01001

Figure 9 Boundary hierarchical graph

Therefore, this method can be used to detect only the outermost contour which was not surrounded by holes (such as c0 in Figure 9). This method was used to detect the outermost contours in the binary image, and the result is shown in Figure 10. There were not only the ridge contour, but also many other useless contours. According to the characteristics that the ridge contour area was the largest, the ridge contour was screened, as shown in Figure 11. The ridge contour was stored as a set of points.

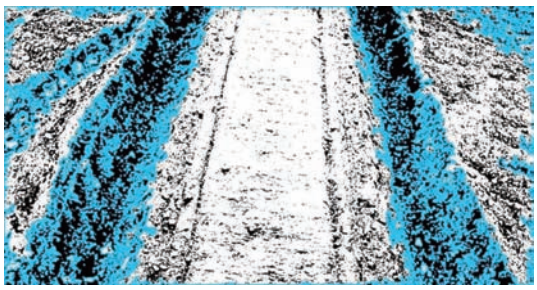

Note: the blue areas are the contours screened by the proposed boundary detection method.

Figure 10 Result example of outermost contours detection in binary image

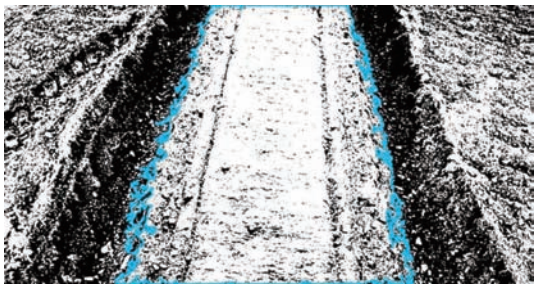

Note: The blue lines represent the screened ridge contour area.

Figure 11 Result example of the screened ridge contour area

2.5 Ridge center line extraction method

In order to extract the ridge center line, the ridge boundaries need to be extracted first. When the ridge contour is known, the Hough transform method[23] is usually used to extract lines. When the ridge contour completely reflected the ridge boundaries and the interior was not messy, the Hough transform method could successfully identify the ridge boundaries. However, when the ridge contour lacked some boundary information or the internal texture feature was obvious, the Hough transform method could not correctly identify the ridge boundaries, as shown in Figure 12.

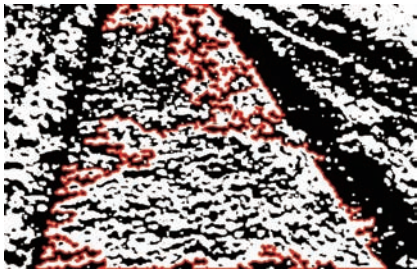

a. Ridge contour

b. Theta=75

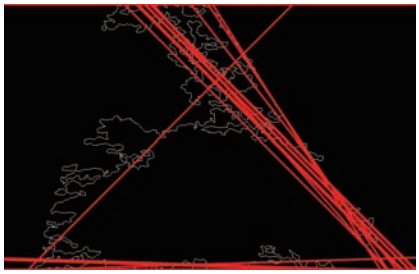

c. Theta=60

Note: In Figure 12a, the red points represent the ridge contours that have been detected. In Figures 12b and 12c, the red lines indicate the results of the Hough transform at different Theta values. Theta denotes the angle in degrees between the *x*-axis and the line to be detected.

Figure 12 Result example of Hough transform identification

In order to extract ridge boundaries correctly from irregular ridge contours, an approximate quadrilateral method was proposed in this study. The shape of the ridge is approximately quadrilateral, and the ridge boundaries can be regarded as the two long sides of the quadrilateral. If the coordinates of the four endpoints of the ridge quadrilateral are known, the linear equation of the ridge boundaries can be calculated. The four endpoints are located on the ridge contour stored in a point set. Therefore, the endpoints can be filtered out in the ridge contour point set. Because of the large number of ridge contour points, it took a long time to filter the endpoints. In order to shorten the running time, the contour convex hull method was used to convex hull the ridge contour and obtain the ridge convex hull contour point set. The four endpoints were filtered from the convex hull contour point set by the approximation quadrilateral method. The flow chart of the approximation quadrilateral method is shown in Figure 13.

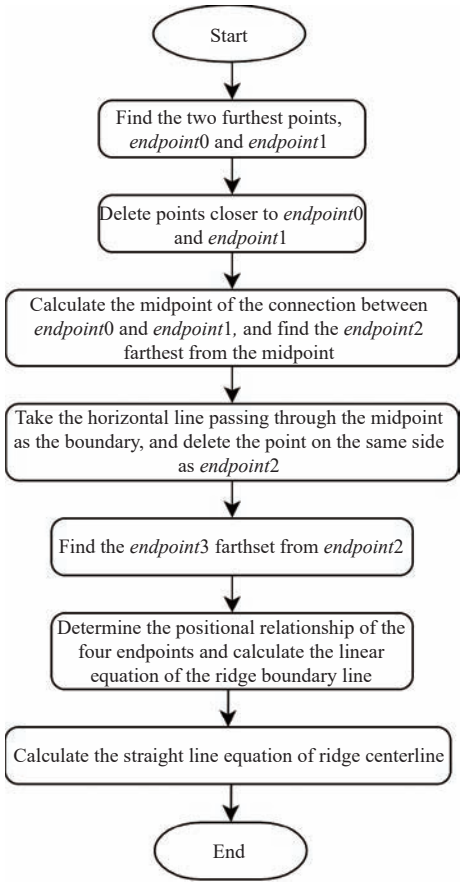

Figure 13 Flow chart of approximation quadrilateral method

The specific implementation method of approximating quadrilateral was elaborated as follows:

1) The black line in Figure 14 is the ridge convex hull contour. Firstly, the distance between all points in the ridge convex hull contour point set was calculated and the two farthest points were found, that is, the two endpoints at the diagonal position of the quadrilateral. The two endpoints were defined as endpoint0 and endpoint1, respectively, the distance between endpoint0 and endpoint1 was defined as max_dist, and the midpoint of the line connected by endpoint0 and endpoint1 was defined as midpoint. The red line in Figure 14 is the connection between endpoint0 and endpoint1;

2) In order to avoid the points around endpoint0 and endpoint1 interfere with the search of the next endpoint, delete the points in the ridge convex hull contour point set whose distance from endpoint0 or endpoint1 was less than max_dist/10;

3) The distance equation between two points was used to calculate the distance from the point in the ridge convex hull

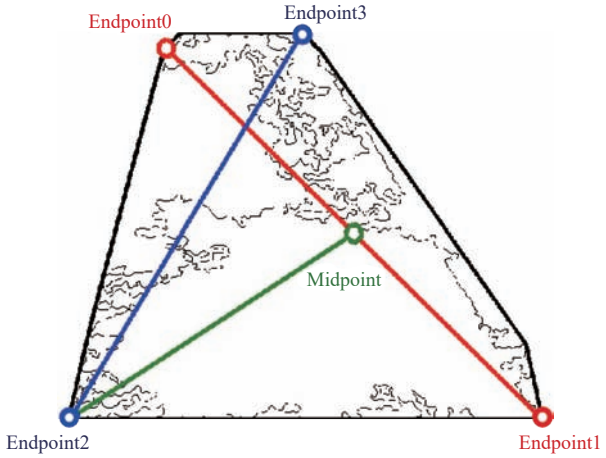

Figure 14 Approximation quadrilateral method

contour point set to the midpoint. The point with the largest distance was regarded as the third endpoint of the quadrilateral, which was defined as endpoint2. The olive green line in Figure 14 is the connecting line between midpoint and endpoint2.

4) Since the fourth endpoint and endpoint2 must be in the diagonal position of the quadrilateral, the fourth endpoint must not be on the same side of the quadrilateral as endpoint2. In order to reduce the number of calculation points and remove the interference of redundant points on finding the fourth endpoint, the coordinates of the points were used to delete the redundant points on the same side as the endpoint2. If the Y coordinate of endpoint2 was less than the Y coordinate of the center point, the points in the ridge contour point set whose Y coordinate was less than the Y coordinate of the center point were deleted. If the Y coordinate of endpoint2 was greater than the Y coordinate of the center point, the points in the ridge contour point set whose Y coordinate was greater than the Y coordinate of the center point were deleted.

5) The point furthest from endpoint2 was found as the fourth endpoint of the quadrilateral, which was defined as endpoint3. The blue line in Figure 14 is the connection between endpoint2 and endpoint3.

6) The positional relationship of the four endpoints in the quadrilateral was determined by the coordinates of the four endpoints. First, the two endpoints whose Y coordinate was less than the midpoint Y coordinate were taken as the upper group, and the other two endpoints were regarded as the bottom group. Then, the endpoints in the bottom and upper groups were sorted respectively according to the X coordinate value from small to large. The line between the first point in the bottom group and the first point in the upper group was the left boundary of the ridge. The line between the second point in the bottom group and the second point in the upper group was the right boundary of the ridge.

7) The linear equation of the ridge boundaries was known, and the ridge center line equation was calculated by the angular bisector equation.

3 Results

3.1 Navigation line recognition effect

The images in Figure 15 display different conditions of the ridge, such as light-colored, dark, film-covered, and sunny ridges. The method proposed by this study was used to recognize the navigation lines of the ridges, and its recognition effects. There are 3 lines of images in Figure 15. The first line of images displays the original photo of the ridge. The second line of the images shows the processing procedure of the images by the proposed navigation line recognition method. Moreover, the third line of the images

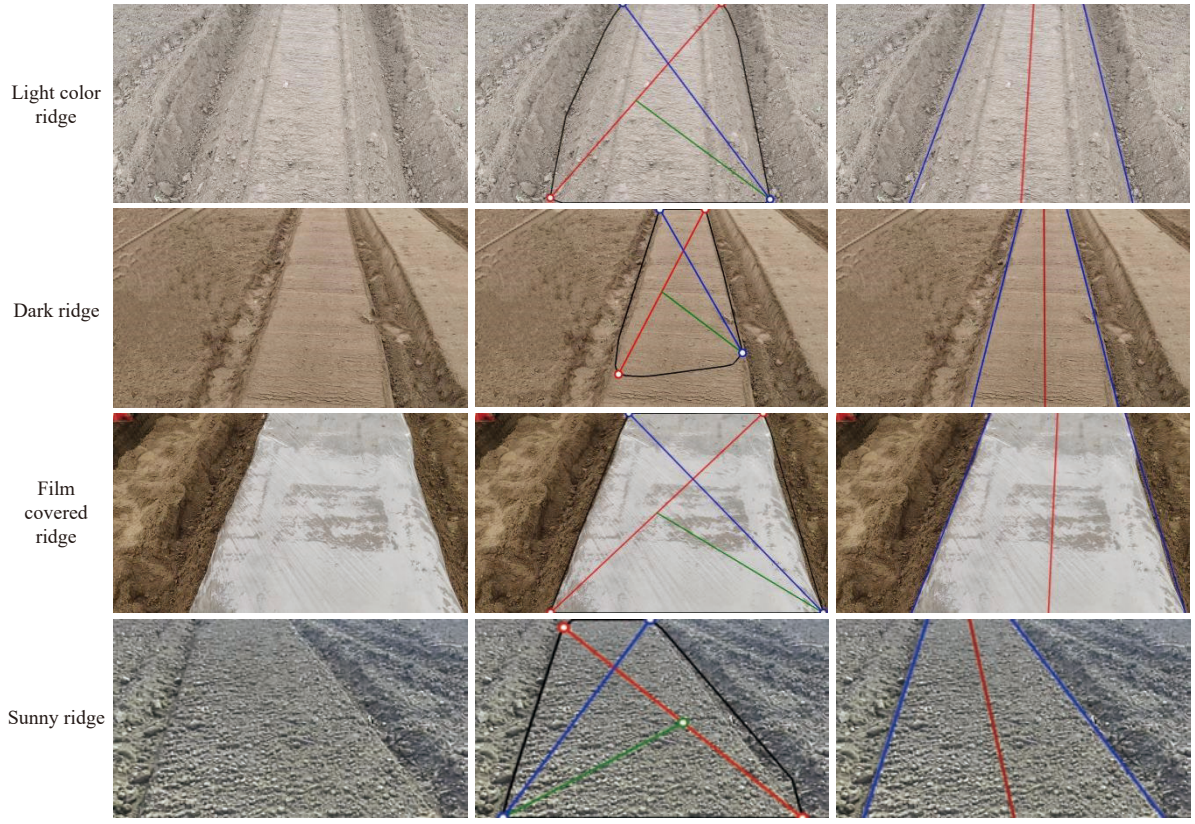

Note: In the image of the detected line, the blue line is the detected edge line of the ridge. Furthermore, the red line is the detected center line of the ridge, and the center line is used as the navigation line.

Figure 15 Navigation line recognition effects

demonstrates the recognized navigation lines. The blue lines mark the detected edges of the ridge. These lines have been identified by the algorithm as the outer boundaries of the ridge structure. The red line represents the detected center line of the ridge, which has been computed based on the detected edges. The center red line is crucial as it provides a path for navigation, indicating where agricultural machinery should be guided for tasks such as planting or spraying applications. The clarity and accuracy of the blue and red lines across various ridge conditions suggest that the method is robust and capable of performing well in different environmental settings, which is essential for real-world agricultural applications.

3.2 Evaluation index

In order to quantitatively analyze the accuracy of the navigation line recognition method, the line obtained by manually connecting the midpoint of the proximal ridge width and the midpoint of the distal ridge width in the original image was used as the benchmark navigation line. The proximal ridge width and the distal ridge width were marked as L_b and L_a, respectively. The unit of both of the L_b and L_a is m. The recognition navigation line obtained by this method was compared with the benchmark navigation line. The deviation angle was marked as $\Delta\theta$ (°) and the deviation distance was marked as Δx (m). The angle between the recognition navigation line and the benchmark navigation line was taken as the deviation angle. The difference between the X coordinate of the far end of the recognition navigation line and the benchmark navigation line was Δx_a (m). The difference between the X coordinate of the near end of the recognition navigation line and the benchmark navigation line was Δx_b (m). The deviation distance between the recognition navigation line and the benchmark navigation line was calculated as follows:

$$\Delta x = (|\Delta x_a| + |\Delta x_b|)/L_b \tag{9}$$

The deviation diagram between the recognition navigation line and the benchmark navigation line is shown in Figure 16. The black line is the benchmark navigation line, the red line is the recognition navigation line, and the blue line is the recognition ridge boundary line.

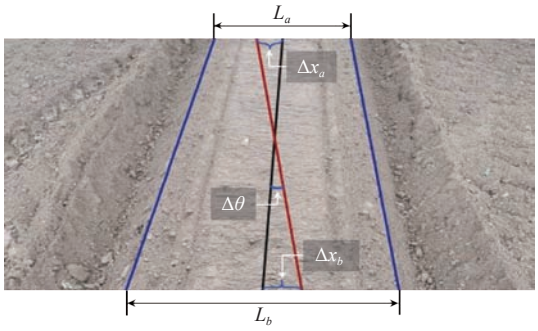

Note: The black line is the benchmark navigation line, the red line is the recognition navigation line, and the blue line is the recognition ridge boundary line.

Figure 16 Deviation diagram between the recognition navigation line and the benchmark navigation line

In order to assess the accuracy and efficiency of the proposed navigation method, this study took the recognition success rate, running time, deviation angle, and deviation distance as the evaluation indexes of the method.

3.3 Navigation line recognition result

The recognition result of the navigation line is listed in Table 2. The accuracy evaluation of navigation line recognition is listed in Table 3. The recognition success rates of the four types of ridge were more than 97%, and the recognition success rates of film-covered ridge and light ridge were 100%. The algorithm running time of each image was within 0.3 s, the deviation angle was less than 1°, and the deviation distance was less than 0.03 L_b, which can meet the actual requirements.

Table 2 Navigation line recognition result

Dataset	Success Rate/%	Average running time/s
Light ridge	100	0.264±0.021
Dark ridge	97.5	0.202±0.017
Film covered ridge	100	0.136±0.012
Sunny ridge	98.7	0.247±0.016

Table 3 Accuracy evaluation of navigation line recognition

Dataset	Deviation angle		Deviation distance	
	MAE/(°)	RMSE/(°)	MAE/L_b	RMSE/L_b
Light ridge	0.9404	0.4527	0.0203	0.0268
Dark ridge	0.6119	0.2688	0.0181	0.0229
Film covered ridge	0.2388	0.1604	0.0044	0.0047
Sunny ridge	0.3684	0.2176	0.0216	0.0242

4 Discussion

According to the navigation line recognition results, the method proposed in this study can be applied to four types of ridge. Due to the color difference between the ridge and furrow being large and the boundary line of the ridge being obvious in the film-covered ridge image, the recognition result of ridge contour is more accurate. Then the recognition success rate of the film-covered ridge image is the highest and the recognition error is the smallest. The dark ridge images are taken from a far field of vision. Compared with the ridge image taken from near-field, the ridge area occupies a smaller proportion in the image, and the background area is larger. Therefore, when screening the ridge contour, it is more likely that the contour of the largest area is not the correct ridge contour. So the recognition success rate of the dark ridge images decreases.

The recognition success rate of this method for four types of ridge was more than 97%. Takagaki et al.[17] proposed the furrow line recognition method, and the recognition success rate for unshaded ridges was 87%. By comparison, the recognition success rate of the proposed method in this study is at least 8% higher than that of other methods.

The furrow line recognition method proposed by Takagaki et al.[17] for ridge images with shadows in sunlight had a success rate of 100%. The gray histogram of the ridge image with shadow shows bimodal distribution, and the maximum between-class variance method (Otsu) can be used to segment the shadow part of the image. There is no shadow in the ridge images collected in this study. The gray histogram of the ridge images without shadow is shown in Figure 17. The gray histogram is not bimodal distribution. The binary image obtained by using the Otsu method to segment the gray image is shown in Figure 18. Using this method cannot successfully segment the ridge part and this method does not apply to the ridge without shadow.

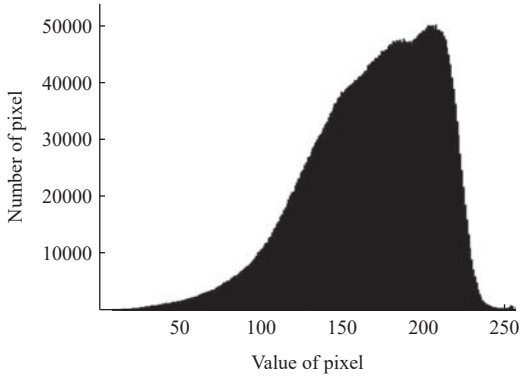

Figure 17 Gray histogram of the ridge images without shadow

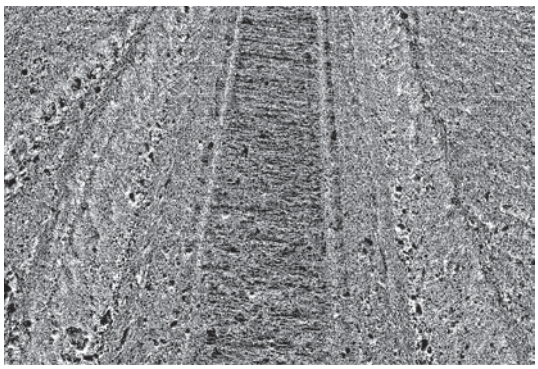

Figure 18 Binary image obtained by the Otsu method to segment the gray image

5 Conclusions

In order to solve the problem that there is no crop reference on the ridge surface when machine vision navigation is used for the transplanter and the seeder operation, a navigation line recognition method based on the ridge color feature is proposed in this study. This method can effectively identify navigation lines for ridges with different colors and textures. It provides technical support for the autonomous navigation of the machinery operating on the ridge without crops such as transplanters and planters. The main conclusions are described as follows:

1) In this study, a gray reconstruction method was used to enlarge the small color difference between the ridge and the furrow itself. Then the threshold segmentation method could calculate the optimal threshold real-timely for gray image segmentation and obtain the binary image. Based on the binary image, the contour detection method, which had the topological analysis ability, could detect the ridge contour. Finally, the approximate quadrilateral method recognized the ridge center line according to the ridge contour and took the ridge center line as the navigation line.

2) The region of interest was calculated and extracted based on the response time and the forward speed of the machine. The forward distance within the time of lag in machine response was taken as the distance from the lower boundary of the region of interest to the lower boundary of the image. This method solved the problem that the recognition navigation line was not the actual navigation line when the machine made a steering response in the navigation process. At the same time, the range of image recognition was reduced and the running time of the navigation line recognition method was shortened.

3) The navigation line recognition method proposed in this paper was experimentally verified. The experimental results showed that the method could successfully recognize the navigation line of the machinery working on the ridge with different colors and textures. The recognition success rate was more than 97%, which was at least 8% higher than that of furrow recognition methods. The running time of each image was less than 0.3 s, which meets the actual navigation requirements.

Acknowledgements

This research was financially supported by the Construction of Technical System of Green Leafy Vegetable Industry in Shanghai—Development and application of key technologies for high-density transplanting of green leafy vegetables [Shanghai Agricultural Science and Production (2023) No.2], the Jiangsu Provincial Key Research and Development Program (Grant No. BE2021342) and A Project Funded by the Priority Academic Program Development of Jiangsu Higher Education Institutions (No. PAPD-2023-87).

[References]

[1] Liu X L, Wang Y D, Yan X Q, Hou H Z, Liu P, Cai T, et al. Appropriate ridge-furrow ratio can enhance crop production and resource use efficiency by improving soil moisture and thermal condition in a semi-arid region. Agricultural Water Management, 2020; 240: 106289.

[2] Sarker K K, Hossain A, Timsina J, Biswas S K, Kundu B C, Barman A, et al. Yield and quality of potato tuber and its water productivity are influenced by alternate furrow irrigation in a raised bed system. Agricultural Water Management, 2019; 224: 105750.

[3] Galati A, Sabatino L, Prinzivalli C S, D'Anna F, Scalenghe R. Strawberry fields forever: That is, how many grams of plastics are used to grow a strawberry? Journal of Environmental Management, 2020; 276: 111313.

[4] Han L H, Xiang D Q, Xu Q Q, Du X W, Ma G X, Mao H P. Development of simplified seedling transplanting device for supporting efficient production of vegetable raw materials. Applied Sciences-Basel, 2023; 13(18): 10022.

[5] Tang Z, Wang H, Liu S, Lu D, Tang Y. Development of structure and control system of self-propelled small green vegetables combine harvester. Agricultural Science and Technology, 2023; 25(5): 1045–1058.

[6] Ahmad F, Adeel M, Qiu B J, Ma J, Shoaib M, Shakoor A, et al. Sowing uniformity of bed-type pneumatic maize planter at various seedbed preparation levels and machine travel speeds. Int J Agric & Biol Eng, 2021; 14(1): 165.

[7] Fang H M, Niu M M, Zhu Z B, Zhang Q Y. Experimental and numerical investigations of the impacts of separating board and anti-blocking mechanism on maize seeding. Journal of Agricultural Engineering, 2022; 53(1): 1273.

[8] Huang W Y, Ji X, Wang A Z, Wang Y F, Wei X H. Straight-line path tracking control of agricultural tractor-trailer based on fuzzy sliding mode control. Applied Sciences-Basel, 2023; 13(2): 872.

[9] Ding C, Ding S H, Wei X H, Mei K Q. Output feedback sliding mode control for path-tracking of autonomous agricultural vehicles. Nonlinear Dynamics, 2022; 110(3): 2429-2445.

[10] Opiyo S, Okinda C, Zhou J, Mwangi E, Makange N. Medial axis-based machine-vision system for orchard robot navigation. Computers and Electronics in Agriculture, 2021; 185: 106153.

[11] Bonadies S, Andrew Gadsden S. An overview of autonomous crop row navigation strategies for unmanned ground vehicles. Engineering in Agriculture, Environment and Food, 2019; 12(1): 24–31.

[12] Ospina R, Noguchi N. Simultaneous mapping and crop row detection by fusing data from wide angle and telephoto images. Computers and Electronics in Agriculture, 2019; 162: 602–612.

[13] Chen J Q, Qiang H, Wu J H, Xu G W, Wang Z K. Navigation path extraction for greenhouse cucumber-picking robots using the prediction-point Hough transform. Computers and Electronics in Agriculture, 2021; 180: 105911.

[14] Rabab S, Badenhorst P, Chen Y-P P, Daetwyler H D. A template-free machine vision-based crop row detection algorithm. Precision Agriculture, 2021; 22: 124–153.

[15] Hamuda E, Mc Ginley B, Glavin M, Jones E. Automatic crop detection under field conditions using the HSV colour space and morphological

operations. Computers and Electronics in Agriculture, 2016; 133: 97–107.

[16] Morio Y, Teramoto K, Murakami K. Vision-based furrow line detection for navigating intelligent worker assistance robot. Engineering in Agriculture, Environment and Food, 2017; 10(2): 87–103.

[17] Takagaki A, Masuda R, Iida M, Suguri M. Image processing for ridge/furrow discrimination for autonomous agricultural vehicles navigation. IFAC Proceedings Volumes, 2013; 46(18): 47–51.

[18] Gu X B, Cai H J, Zhang Z T, Fang H, Chen P P, Huang P, et al. Ridge-furrow full film mulching: An adaptive management strategy to reduce irrigation of dryland winter rapeseed (*Brassica napus* L.) in northwest China. Agricultural and Forest Meteorology, 2019; 266-267: 119–128.

[19] Otsu N. A threshold selection method from gray-level histogram. IEEE Transactions on Systems, Man, and Cybernetics, 1979; 9(1): 62–66.

[20] Sauvola J, Pietikäinen M. Adaptive document image binarization. Pattern Recognition, 2000; 33(2): 225–236.

[21] Canny J. A computational approach to edge detection. IEEE Transactions on Pattern Analysis and Machine Intelligence. 1986; 8(6): 679–698. doi: 10.1109/TPAMI.1986.4767851.

[22] Suzuki S, Abe K. Topological structural analysis of digitized binary images by border following. Computer Vision, Graph, and Image Processing, 1985; 29(3): 396.

[23] Duda R O, Hart P E. Use of the Hough transformation to detect lines and curves in pictures. Communications of the ACM, 1972; 15(1): 11–15.